Experimental geoecology

Karaseva O.N.[1], Khanin D.A.[1,2], Lakshtanov L.Z.[1] Cadmium adsorption on talc (kinetics and equilibrium). *UDC 541.18 + 628.316.12*

[1]D.S. Korzhinskii Institute of Experimental Mineralogy RAS, Chernogolovka, Russia; [2]Geol Faculty, Moscow State University State University olga@iem.ac.ru

Abstract. The adsorption of cadmium ions on the surface of natural talc was studied. The dependences of the adsorption value on the pH of the solution at 25^0 C were obtained. It was shown that the maximum absorption of cadmium from the solution occurs at pH 7–8. Adsorption is most intense in the first 5 min, the adsorption equilibrium is established approximately 40 min after the mineral/solution contact. The contribution of the stage of chemical interaction of cadmium ions with the talc surface to the overall rate of the process was established, which is confirmed by the agreement between the experimental data and the pseudo-second-order kinetic model. Adsorption isotherms are most adequately described by the Freundlich model, which indicates the heterogeneity of the surface adsorption centers with different energies. The effective sorption of cadmium ions by talc makes it possible to use talc as a sorbent for the purification of natural and industrial wastewater in a wide pH range.

***Keywords**: adsorption, cadmium, talc, kinetics, adsorption isotherms*

Cadmium Cd(II) is one of the most toxic heavy metals that can accumulate in the human body and cause various diseases of the kidneys, bones and lungs (Mehta et al., 2015; Mehta et al., 2016; Paesano et al., 2020; Sun et al., 2020). Cadmium is typically present as Cd^{2+} in the environment, and its adsorption to environmentally relevant substrates can reduce its concentration and mobility in aquatic systems. In our work, we attempted a comprehensive study of cadmium adsorption on talc with further conclusions on the effectiveness of using talc as a barrier to limit cadmium mobility. To understand the mechanisms of cadmium adsorption on talc, the kinetics and equilibrium of adsorption were studied over a wide range of pH and cadmium concentration.

Natural talc from the Shabrovsky deposit in the Middle Urals was used as an adsorbent. The mineral composition was confirmed using X-ray phase analysis on a D2 Phaser diffractometer (Bruker). According to the results of microprobe analysis, the average formula of talc is $(Mg_{2.85}Al_{0.04}Fe_{0.01})_{2.90}Si_{4.02}O_{10}(OH)_2$. Talc contains a minor admixture of Al_2O_3 up to 1.7 wt.%, FeO up to 0.5 wt.%, the content of Ca, V, Cr, Mn, Ni, Co, Zn is below the detection limit.

The preparation of talc powder with a particle size of 30 - 100 μm is described in detail in the work of Karaseva et al. (2024). The specific surface area of talc was measured by the low-temperature BET method for nitrogen adsorption using a QUADRASORB SI sorption analyzer (Federal Research Center for Problems of Chemical Physics and Medicinal Chemistry of RAS) and was 6.3 m^2/g.

The dependence of Cd^{2+} adsorption on talc on the pH of the solution was studied using potentiometric titrations at 25^{0}C. To do this, 100 ml of 0.01 M NaCl were placed in a sealed thermostatted cell, into the holes of the lid of which a combined electrode and a tube for supplying argon were inserted, 2 ml of 0.01 M HCl and a weighed portion of talc weighing 0.2–1.0 g were added. With vigorous stirring of the suspension and after pH = 3.9 – 4.1, an aliquot of 1 mM solution containing Cd^{2+} (I=0.01 M) was added. The initial concentration of cadmium in the solution ranged from 0.1 to 10 μmol/l. After 40 minutes, an aliquot of the suspension under study was taken and titration was performed by adding 0.01 M NaOH with simultaneous sampling at 40-minute intervals. As will be shown below, during this time the adsorption equilibrium is established. During the experiment the cell was purged with argon to prevent atmospheric carbon dioxide from entering.

When studying the kinetics of adsorption of cadmium ions on the surface of talc, 100 ml of 0.01 M NaCl were placed in a thermostatted cell, 0.5 g of talc was added, the solution was brought to the desired pH in the range from 6 to 8.5 using HCl or NaOH with constant stirring, and an aliquot of the $Cd(NO_3)_2$ solution was introduced. The initial concentration of cadmium in the solution was set from 10-7 to 10-5 M. Samples were taken at certain time intervals after the start of phase contact: after 2, 20, 40 and 120 minutes.

The concentration of Cd in the solution after centrifugation was measured by atomic absorption spectrometry. The relative error of the method was 5%.

Langmuir and Freundlich models were used to describe adsorption isotherms and calculate adsorption equilibrium parameters (Douven et al., 2015; Paez et al., 2011). To describe the kinetic laws of adsorption, the pseudo-second-order equation of Ho and McKay (1999) was used, which can be represented in integrated form as follows:

$$\frac{t}{q_t} = \frac{1}{kq_e^2} + \frac{t}{q_e} \quad (1),$$

where k is the rate constant, g/mg min, where q_e and q_t are the amount of metal sorbed at equilibrium and over a certain period of time t (min), mg/g.

The composition of the solution and the saturation indices were calculated using the PHREEQC program (Parkhurst and Appelo, 1999).

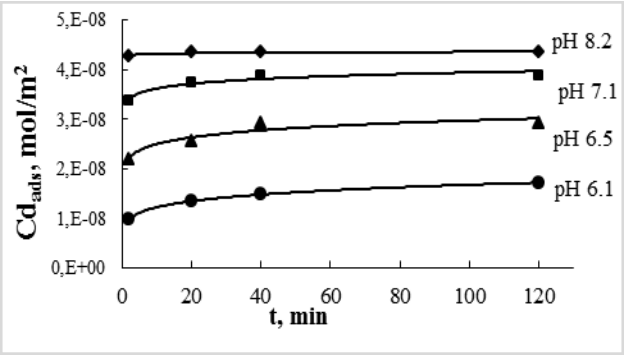

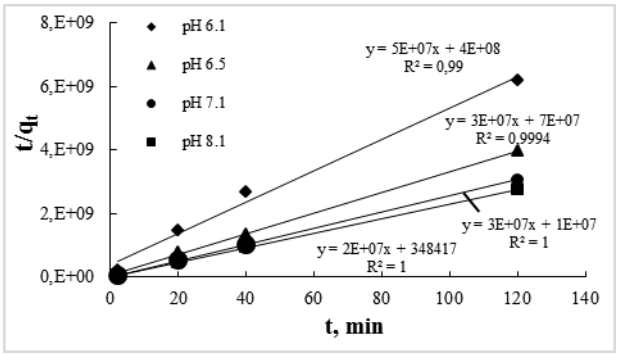

Fig. 1. Kinetics of cadmium adsorption on talc at different pH of the solution. Initial concentrations of cadmium ions 0.97–1.33 μmol/L, T = 25^{0}C.

Fig. 2. Kinetics of adsorption of Cd^{2+} ions in the coordinates of the pseudo-second-order equation. T= 25 ^{0}C**.**

Fig. 1 shows the kinetic curves of cadmium ion adsorption on talc as a function of the amount of absorbed cadmium (Cd_{ads}, mol/m^2) versus time (t, min) in the pH range of 6 - 8. High-speed adsorption of Cd^{2+} occurs in the first 1-5 minutes, and equilibrium is reached approximately 40 - 60 minutes after the start of mineral/solution contact. In this regard, when conducting acid-base titrations of the talc surface, sampling and introducing a new portion of the alkali solution were carried out every 40 minutes. To describe the contribution of chemical interaction to the overall rate of the process, a pseudo-second-order reaction model was used (Ho, McKay, 1999), which allows for sorbate–sorbent interactions, as well as intermolecular interactions of adsorbed particles. If the pseudo-second-order rate kinetics model (equation 1) is applicable to the sorption process, then the plot in the coordinates "t/qτ – t" should have a linear dependence, from which qe and k can be calculated using the slope tangent and the free term of equation (1) (Khamizov, 2020).

As can be seen in Fig.2, the obtained dependences are linear at all pH values and over the entire range of adsorption process times. Based on the obtained graphical dependencies (Fig. 2), the rate constants of the process k and the values of equilibrium adsorption qe were calculated. Experimental data on the kinetic adsorption of Cd^{2+} under natural conditions and the results of the calculations are presented in Table 1. It should be noted that the calculated values of qe give good agreement with the experimental data. High values of the correlation coefficients ($R^2 \geq 0.99$; Table 1) and the linear dependence (Fig. 2) allow us to judge in favor of the applicability of the pseudo-second-order model for describing the chemical stage of the adsorption process, as well as for the possibility of taking into account intermolecular interactions in the "Cd^{2+} - talc" system.

Table 1. Kinetic parameters of the adsorption process of cadmium ions

pH	Initial concentration Cd, *10^{-8}, mol/m^2	Equilibrium value of adsorption q_e *10^{-8}, mole/m^2		κ, m^2/mol min	R^2
		experiment	calculation		
6.1	3.20	1.94	2.0	6.3 · 10^6	0.99
6.5	3.73	3.01	3.33	1.3 ·10^7	0.99
7.1	4.26	3.90	3.33	9.0 ·10^7	1.0
7.5	4.0	3.84	3.33	2.3 ·10^8	1.0
8.1	4.36	4.35	5.0	1.1 · 10^9	1.0

Experimental data obtained during acid-base titrations of talc suspension, related to the range 7 < pH < 8, were used to describe adsorption isotherms and calculate adsorption equilibrium parameters using the Langmuir and Freundlich equations. The process of cadmium adsorption on talc is not described by the Langmuir model, as evidenced by the low values of the correlation coefficients R^2 (0.6 – 0.8). Fig. 3 shows the adsorption isotherms of cadmium ions from aqueous solutions with an initial concentration from 0.1 μmol/l to 10 μmol/l at pH 7–8 on natural talc in logarithmic coordinates of the Freundlich equation. The values of the correlation coefficients R^2 (0.89 and 0.95) indicate an adequate description of the experimental data by the Freundlich isotherm, which suggests that the surface of natural talc contains active centers with different affinity energies for cadmium ions. Cadmium is

likely to adsorb on the Mg-OH plane, forming strong covalent bonds, while adsorption on Si-O centers is associated only with electrostatic attraction with the formation of weak outer-sphere complexes (Pivovarov, 2008; Wang et al., 2023). The constants of the Freundlich equations K_F and n, presented in Table 2, were calculated from the angle of inclination and intersection of the straight axis with the ordinate axis. The value of K_F depends on the pH of the solution, while the parameter 1/n, indicating the change in the adsorption process and the distribution of active centers, remains practically unchanged. The value of 1/n is approximately 0.5, indicating a high affinity of the talc surface to cadmium ions. With an increase in the pH of the solution by 1, the values of K_F increase approximately twofold, which is consistent with the change in cadmium adsorption with an increase in pH.

Table 2. Values of constants in the Freundlich isotherm equations for the adsorption of cadmium ions on talc at 25 ^{0}C.

pH	K_F, mol/m^2 · 10^5	1/n	Correlation coefficient R^2
7	3.43	0.469	0.954
8	6.78	0.461	0.892

The results of the study show that the adsorption equilibrium is described by the Freundlich isotherm, which suggests that the talc surface contains active centers with different affinity energies for cadmium ions. The adsorption equilibrium is established within 40 minutes. The adsorption of cadmium ions on talc follows a pseudo-second-order kinetic model, and the rate-limiting stage of the adsorption process is the chemical interaction between cadmium ions and functional groups on the talc surface with the formation of strong covalent bonds. The effective absorption of cadmium ions by talc makes it possible to use talc as a sorbent for the purification of natural and industrial wastewater in a wide pH range.

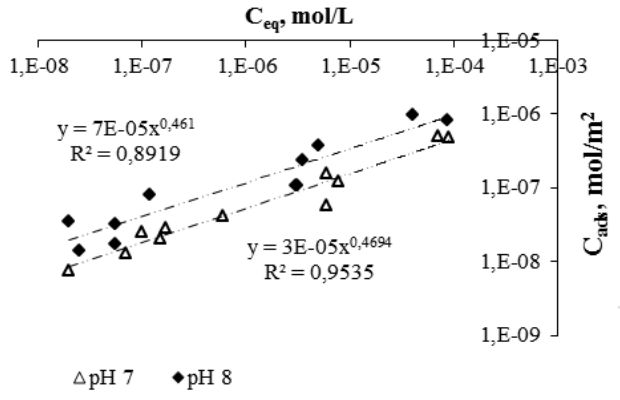

Fig. 3. Adsorption isotherms of cadmium ions on natural talc according to the Freundlich model at 25 ^{0}C.

This study is fulfilled under Research program № FMUF-2022-0003 of the Korzhinskii Institute of Experimental Mineralogy

References

Karaseva O., Lakshtanov L., Khanin D. Effect of pH, CO_2, and organic ligand on the kinetics of talc and lizardite dissolution // Geochemistry International 2024. V.69. № 4. P. 393–403.

Khamizov R.. On the kinetic equation of pseudo-second order in sorption processes // Journal of Physical Chemistry 2020. V 94. № 1. P. 125–130.

Douven S., Paez C., Gommes C. The range of validity of sorption kinetic models // Journal of Colloid and Interface Science 2015. V. 448. P. 437-450.

Ho Y.S., McKay G. Pseudo-second order model for sorption processes // Process Biochemistry 1999. V. 34. P. 451–465.

Mehta V., Basu H., Singhal R., et al. Simple and sensitive colorimetric sensing of Cd^{2+} ion using chitosan dithiocarbamate functionalized gold nanoparticles as a probe // Sensors and Actuators B: Chemical 2015. V. 220. P. 850-858.

Mehta J., Bhardwaj S., Bhardwaj N., et el. Progress in the biosensing techniques for trace-level heavy metals // Biotechnology Advances 2016. V.34. P. 47-60.

Paesano L., Marmiroli M., Bianchi M., et el. Differences in toxicity, mitochondrial function and miRNome in human cells exposed in vitro to Cd as CdS quantum dots or ionic Cd // Journal of Hazardous Materials 2020. V.393. P. 1-15.

Paez C., Lambert S., Poelman D., et al. Improvement in the methylene blue adsorption capacity and photocatalytic activity of H_2 -reduced rutile-TiO_2 caused by Ni(II)porphyrin preadsorption // Applied Catalysis B: Environmental 2011. V. 106. P. 220–227.

Parkhurst D. and Appelo C. User's Guide to PHREEQC (Version 2)—A Computer Program for Speciation, Batch-Reaction, One-Dimensional Transport, and Inverse Geochemical Calculations // In U.S. Geological Survey, Water Resources Investigations Report 99-4259; Washington DC. 1999. P.327.

Pivovarov S. Adsorption of ions onto amorphous silica: Ion exchange model // Journal of Colloid and Interface Science 2008. V. 319. P. 374–376

Ruyter-Hooley M., Johnson B., Morton D., et al. The adsorption of myo-inositol hexaphosphate onto kaolinite and its effect on cadmium retention // Applied Clay Science 2017. V. 135. P. 405—413.

Sun Y., Ye H., Wei Z.,et al. Root cell walls and phytochelatins in low-cadmium cultivar of Brassica parachinensis // Pedosphere 2020. V.30. P. 426-432.

Wang Z., Tian H., Liu J., et al. Cd(II) adsorption on earth-abundant serpentine in aqueous environment: Role of interfacial ion specificity // Environmental Pollution 2023. V. 331. 121845.

Karaseva O.N.[1], Khanin D.A.[1,2], Lakshtanov L.Z.[1] **Changes in the specific surface area and sorption properties of ferrihydrite during its recrystallization**. *UDC 541.183 + 628.316*

[1]D.S. Korzhinskii Institute of Experimental Mineralogy RAS, Chernogolovka, Russia; [2]Geol Faculty, Moscow State University State University; olga@iem.ac.ru

Abstract. This study investigates the sorption properties of ferrihydrite (Fh), an effective natural sorbent for the immobilization of heavy metals and radionuclides, using zinc and strontium as model elements. A key sorption characteristic—the specific surface area of ferrihydrite aged from 2 hours to 15 days—was calculated based on proton adsorption data obtained via potentiometric acid-base titration. The effects of recrystallization temperature and aging time on the efficiency of metal ion immobilization were systematically evaluated. A fundamental difference in the interaction mechanisms between the cations and the solid phase was established: the decrease in aqueous Sr^{2+} concentration is driven primarily by adsorption, whereas for Zn^{2+}, the governing process is structural incorporation into the solid phase. An elevated temperature (75 °C) enhances both strontium adsorption and zinc incorporation. These findings are crucial for accurately predicting the migration and long-term fate of toxic elements at industrial and radioactive waste disposal sites.

***Keywords**: ferrihydrite, specific surface area, coprecipitation, adsorption, zinc, strontium*

Introduction. Ferric iron compounds play a critical role in regulating the mobility and concentration of trace elements in natural aquatic and terrestrial systems. Ferrihydrite (Fh), a poorly crystalline iron oxyhydroxide widely distributed in soils, sediments, and surface waters, possesses a high specific surface area. This property makes it one of the most effective natural sorbents for the immobilization of heavy metals and radionuclides.

Due to its nanoscale crystallite size and variable hydration state, the composition of ferrihydrite has been described in the literature using various chemical formulas. Modern structural studies indicate that the idealized formula $Fe_5O_7(OH) \cdot 4H_2O$ is the most robust from a crystal-chemical perspective, as it accurately reflects the elemental ratios within the structure (Michel et al., 2007). In thermodynamic surface complexation modeling (Eynde et al., 2021), the sorbent mass is commonly normalized per mole of iron, adopting a conventional molar mass for the nanoparticles in the range of 96–98 g/mol Fe.

Determining the specific surface area (S_{sp}) of minerals is essential for modeling surface phenomena and accurately predicting sorption processes in the hydrosphere. For ferrihydrite, however, this task presents methodological challenges. Due to its poorly crystalline nature, the specific surface area of Fh is extremely high, ranging from 200 to 1100 m²/g depending on synthesis conditions, temperature, and aging time (Schwertmann & Cornell, 2000). The conventional gas adsorption method (BET) is inapplicable to ferrihydrite because the required drying and degassing steps irreversibly reduce its surface area by a factor of 2 to 4. A robust alternative is to determine S_{sp} via the adsorption of ions or polar molecules directly in an aqueous suspension. In this study, this approach was implemented using potentiometric acid-base titration to measure proton adsorption.

Another critical objective of this study is to elucidate the mechanisms of toxic metal sorption (using zinc and strontium as examples) during the coprecipitation and subsequent recrystallization of ferrihydrite. Zinc and strontium are among the most widespread and hazardous environmental pollutants, entering ecosystems via mining and heavy industrial effluents, municipal solid waste, and radioactive waste disposal. These specific elements were selected because their interaction with Fh is expected to differ significantly, owing to distinct variations in their ionic radii and electron affinities.

Materials and Methods. Ferrihydrite was synthesized by slowly adding 0.5 M NaOH to a 0.1 M iron(III) nitrate solution until the pH reached 7.9–8.2 (Schwertmann & Cornell, 2000). The resulting suspension was quantitatively transferred into a polypropylene centrifuge tube, diluted to 50 mL with distilled water, and incubated in a water bath at 25 °C or 75 °C for a period ranging from 1 hour to 15 days. After the specified aging period, the suspension was centrifuged and washed several times with distilled water. The obtained precipitate was then resuspended in a 0.1 M or 0.01 M NaCl solution, shaken on an orbital shaker for 2 hours, and subsequently titrated with 0.1 M HCl and 0.1 M NaOH solutions. Potentiometric titrations were performed in the pH range of 3.5–10 at temperatures of 25 °C and 75 ± 0.5 °C under an argon atmosphere to exclude the influence of atmospheric CO_2.

To study the interaction of metal ions with ferrihydrite, solutions containing Zn^{2+} and Sr^{2+} were introduced into the initial $Fe(NO_3)_3$ solution prior to Fh synthesis, which was then carried out using the method described above. The resulting suspension was quantitatively transferred into 50 mL polypropylene tubes and incubated in a water bath at 25.0 °C or 75.0 °C. At specified time intervals ranging from 1 hour to 15 days, aliquots of the liquid phase were collected and filtered through a 0.45 μm syringe filter. The concentrations of Zn^{2+} and Sr^{2+} in the filtrate were determined by ICP-MS. The relative analytical error did not exceed 3%.

Results. It is well known that the specific surface area of freshly precipitated ferrihydrite decreases within the first few minutes before stabilizing at approximately 600 m^2/g (Schwertmann & Cornell,

2000). Subsequent structural modifications proceed significantly slower, enabling potentiometric acid-base titrations of the Fh samples. The point of zero charge pH_{pzc} of the surface was determined from the intersection of the titration curves obtained at various ionic strengths, yielding a value of 8.0–8.3 (Fig. 1).

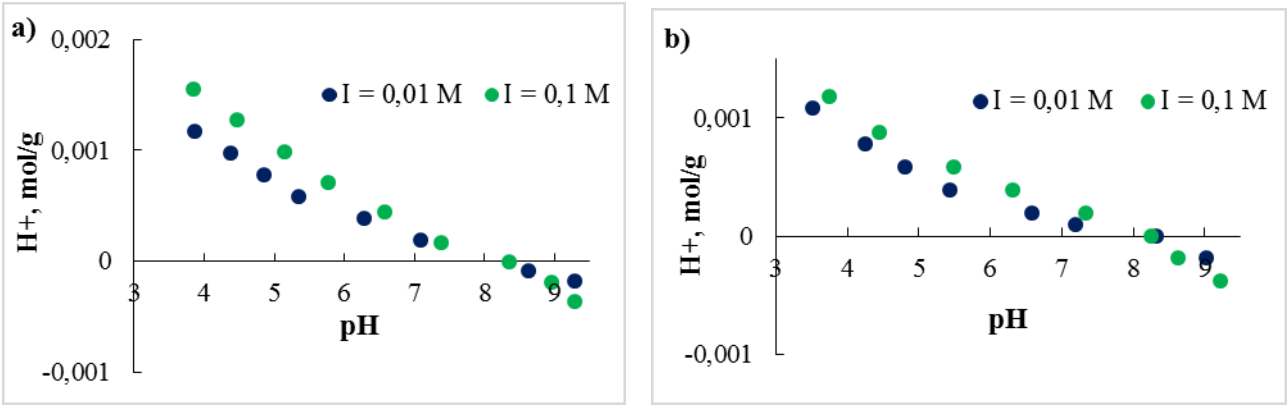

Fig. 1. Proton adsorption on ferrihydrite at various ionic strengths. Fh recrystallization time: (a) 5 days at 25 °C, and (b) 5 hours at 75 °C.

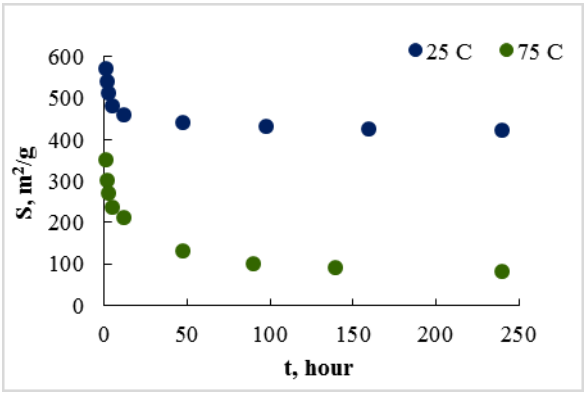

Fig. 2. Evolution of the ferrihydrite specific surface area as a function of aging time.

To determine the temporal evolution of the mineral's specific surface area, titrations were performed on Fh suspensions aged for intervals ranging from 1 hour to 15 days. Using a previously developed surface complexation model (Karaseva et al., 2003) that describes surface acid-base equilibria on hematite at ambient and elevated temperatures, the specific surface area values of ferrihydrite were calculated for aging times spanning 1 hour to 10 days. Based on the assumption that the acid-base properties of the hematite and ferrihydrite surfaces are identical, the calculation model included previously determined surface equilibrium constants, the concentration of active sites (>FeOH), and the specific capacitance of the electrical double layer (Table 1). The specific surface area was calculated as a function of aging time and temperature using the FITEQL computer program; the results are presented in Fig. 2. As can be seen, significant surface area reduction occurs within the first two days, with increasing temperature significantly accelerating this process.

Table 1. Surface acid-base properties of hematite at 25 and 75 °C

Surface reactions	**25 ^{0}C**	**75 ^{0}C**
>FeOH + H^+ = >$FeOH_2^+$ log K_{int}	7.48	7.45
>FeOH = FeO^- + H^+ log K_{int}	9.53	8.1
Specific capacitance, F m^{-2}	1.22	0.83
>FeOH concentration, mmol/L	2.0	2.0
S, m^2/g	4.5	4.5

At 25 °C, one hour after the onset of recrystallization, the specific surface area of iron(III) hydroxide was 570 m²/g, decreasing to approximately 420 m²/g by the 10th day. The recrystallization rate of Fh is significantly higher when the temperature is increased to 75 °C: approximately 2 hours from the start of recrystallization, the specific surface area is 280 m²/g, drops to about 130 m²/g by the end of the second day, and further decreases to 80 m²/g by the 10th day.

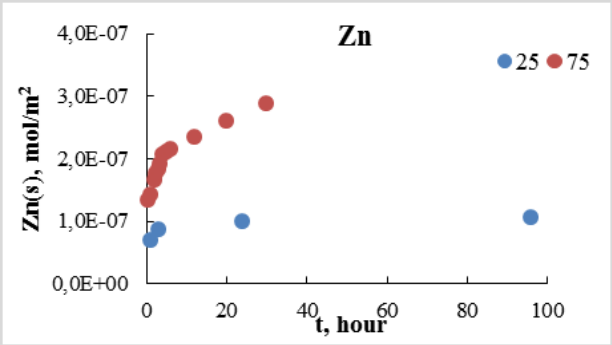

Fig. 3. Sorption of Sr^{2+} and Zn^{2+} during Fh recrystallization at T =25 ^{0}C and pH~8

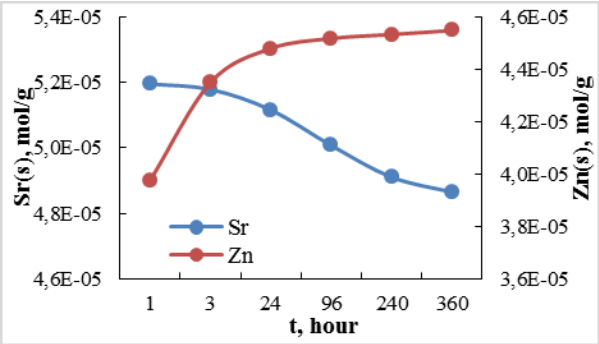

Fig. 4. Sorption Zn^{2+} during Fh recrystallization at T =25 ^{0}C and pH~8

Based on the pH_{pzc} determined above, it can be concluded that the Fh surface is positively charged in natural waters with near-neutral pH values. Accordingly, the binding of metal cations occurs not through electrostatic forces but via chemical interactions (specific adsorption or coprecipitation). In this study, the behavior of zinc and strontium ions during Fh recrystallization was investigated at pH ~ 8 and temperatures of 25 and 75 °C. Under these conditions, Sr^{2+} and Zn^{2+} sorption was found to range from 85% to 97% at 25 °C and exceed 95% at 75 °C. Figure 3 shows the sorption capacities of Sr(s) and Zn(s) (in moles per gram of the solid phase) as a function of Fh recrystallization time. As shown in the graph, strontium sorption decreases over time, whereas zinc sorption increases noticeably. The aging of ferrihydrite leads to a reduction in the specific surface area and, consequently, a decrease in the concentration of adsorption sites (>FeOH) involved in surface complexation reactions. The observed dependence of strontium uptake on the concentration of surface >FeOH groups indicates that surface adsorption is the primary process controlling strontium behavior in the presence of Fh. In the case of zinc, its sorption from the solution increases significantly during ferrihydrite recrystallization. Figure 4 shows that at 75 °C, zinc uptake increases even though the specific surface area decreases faster than at 25 °C. Apparently, in this case, the Fh recrystallization process is accompanied by the co-crystallization entrapment of zinc ions, followed by their incorporation into the crystal lattice of the solid phase, which is favored by the similar ionic radii of Fe^{3+} (0.064 nm) and Zn^{2+} (0.063 nm).

Conclusion. In summary, the specific surface area of ferrihydrite can be successfully determined via acid-base titration based on proton adsorption across any recrystallization time interval. Strontium is not incorporated into the ferrihydrite crystal lattice, primarily due to the significant discrepancy between the ionic radii Sr^{2+} and Fe^{3+}. Consequently, the distribution of strontium between the solid and liquid phases is predominantly controlled by surface adsorption. In contrast to strontium, the intensive recrystallization of Fh promotes zinc immobilization via coprecipitation, driven by the partial isomorphic substitution of iron atoms within the evolving crystal lattice.

This study is fulfilled under Research program № FMUF-2022-0003 of the Korzhinskii Institute of Experimental Mineralogy

References

Karaseva O.N., Ivanova L.I., Lakshtanov L.Z. [Influence of temperature on strontium adsorption on hematite]. *Geokhimiya*, 2003, No. 12, pp. 1–12.

Michel, F. M., Ehm, L., Antao, S. M., Lee, P. L., Chupas, P. J., Liu, G., Strongin, D. R., Schoonen, M. A. A., Phillips, B. L.,Parise, J. B. The structure of ferrihydrite, a nanocrystalline material. *Science*, 2007, *316*(5832), 1726–1729.

Schwertmann, U., Cornell, R. M. Iron Oxides in the Laboratory: Preparation and Characterization (2nd ed.). Wiley-VCH, 2000.

Van Eynde, E., Méndez, J. C., Hiemstra, T., & Comans, R. N. J. Interaction of Zn with ferrihydrite and its cooperative binding in mono- and multi-component systems. *Geochimica et Cosmochimica Acta*, 2022, *320*, 223–237.

Zharikov A.V., Malkovsky V.I. Assessment of actinide colloid transfer in the «Eniseysky» site. *UDC 621.039.7*

IGEM RAS, Moscow (vil@igem.ru)

The main mechanism of radioactive contamination escape from the HLW repository is groundwater transport, into which radionuclides enter as a result of the dissolution of the containment matrix. Moreover, the colloid form of radionuclide transport is considered the most hazardous.Previous experiments have shown that during the leaching (dissolution) of aged Na-Al-P glasses with imitators of long-lived actinides, more than 90 % of the radionuclides pass into the aqueous phase in colloidal form. The size distribution of these particles was

determined by sequentially filtration of the leachate through membranes with progressively reducing pore diameters. Based on the Kozeny–Carman approximation, a theory was developed to estimate the size distribution of pore channels in rocks from measurements of rock sample permeability to gas at various pressures. Such measurements were carried out on samples from the «Yeniseisky» site, taken from core material in the near field of the repository (borehole P12, sampling depth — 496 m). By comparing the size distributions of colloid particles and the pore channel diameters in the samples, it was found that 99.5 % of the colloid particles will be retained mechanically by the rocks of the site.

Keywords: *high level waste, glass matrix, groundwater, radionuclides, colloids, migration, gneiss, granite-gneiss, permeability, mechanical retardation*

One of the most important tasks when choosing a site for the location of an underground depository for high-level radioactive waste (HLW) is to find a massive of monolithic undisturbed low-permeability rocks [Laverov et al., 1991]. However, the experience of geological studies shows that in the upper parts of the earth's crust, up to considerable depths, the rock discontinuities of different scales occur necessarily and there mobile fluids are present: from fracture zones to large faults. The solution of the problem can be to find a block of monolithic rocks with low permeability (because this rock property governs the rate of fluid mass transfer), and the sizes that in case of the probable loss of protective properties by engineering barriers would be sufficient to prevent any pollution escape by groundwater into the biosphere even in the long term. Currently, a project is being considered to create an underground depository in the «Yeniseisky» site located in the Krasnoyarsk region, in the Nizhnekansky massif framing (Fig. 1). This site was selected based on the results of comprehensive geological and geophysical studies, which were compared with a number of alternative sites, including the «Itatsky» and «Kamenny» sites (Fig. 2). The «Yeniseisky» site is mainly composed of Archean granito-gneisses crossed by later dolerite dikes, the discontinuities also occur there Fig. 3.

In the Russian Federation, a significant portion of the HLW intended for disposal in the underground repository is immobilised in a containment matrix based on Na-Al-P glasses. Due to glass-water interaction, up to 90 % of the contained actinides pass into the water in a low-soluble colloidal form. Colloidal particles are poorly sorbed by the rocks and therefore are considered as a most mobile and hazardous form of radionuclide transport. However, these particles can be retained by the rocks mechanically, which is determined by the permeability of the rock matrix and the cross-section of the pore channels [Malkovsky et al., 2022].

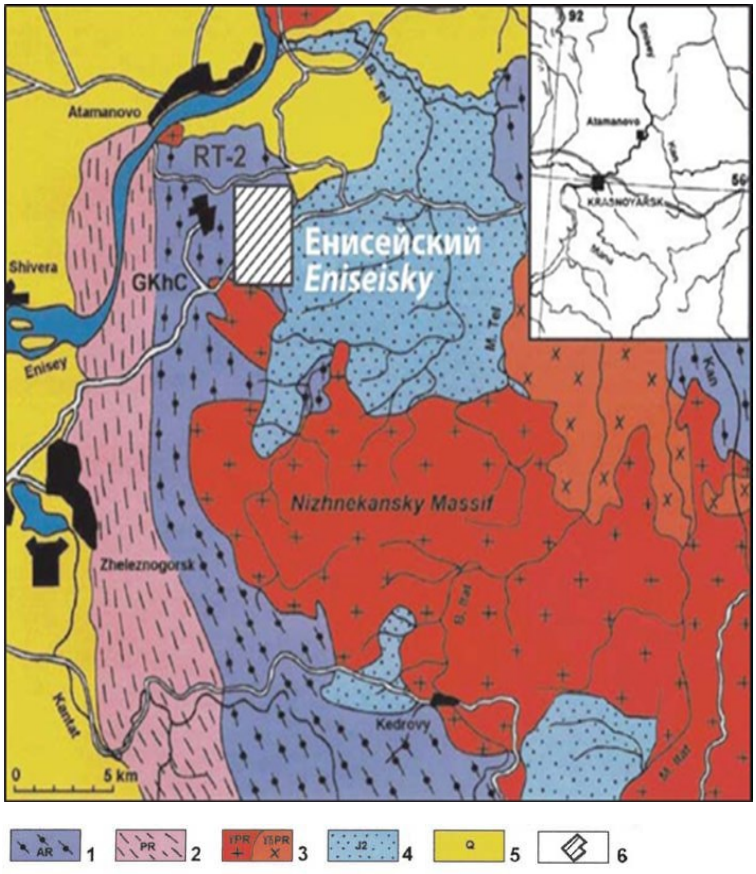

Fig. 1. Geological map of the Krasnoyarsk Mining and Chemical Combine (MCC) area.
1 – gneiss complex;
2 – gneiss-shale complex with amphibolites, marbles and quartzites;
3 – granitoids of the Nizhnekansky complex;
4 – sedimentary rocks;
5 – Quaternary sedimentary deposits.

Fig. 2. The map of the Krasnoyarsk Mining and Chemical Combine (MCC) area and the position of the «Yeniseisky» and alternative sites: «Itatsky» and «Kamenny».

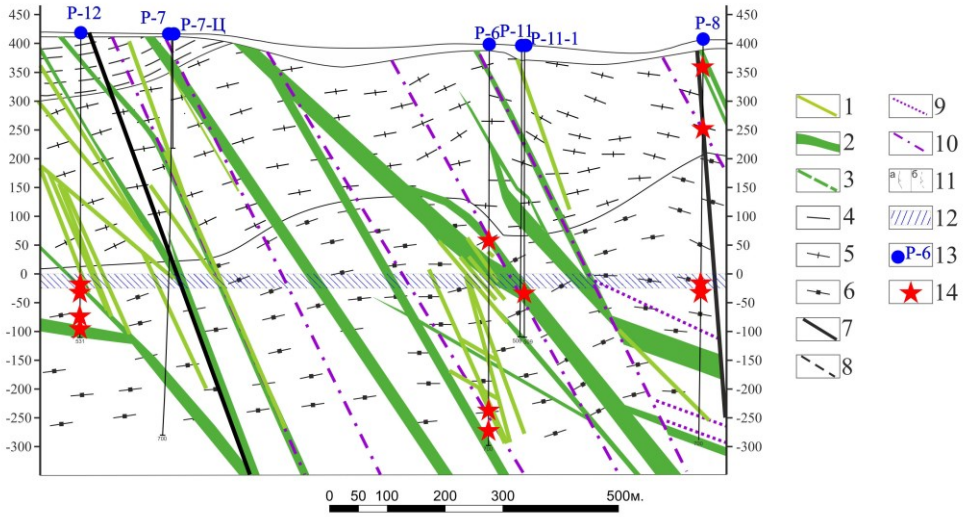

Fig. 3. Geological section of the Yeniseysky site [Minaev et al., 2026].
1 –dikes of gabbro-diabases and diabase porphyries; 2 -3 - dikes of methadolerites and gabbro-diabases; 4 – biotite and bicuspid gneisses and schists with rare interlayers of sillimanite-cordierite shales; 5 – biotite plagiogneisses with rare interlayers of garnet-biotite gneisses and sillimanite-cordierite shales; 6 – biotite-cordierite gneisses and crystalline schists with layers of biotite and biotite-hypersthenic gneisses; 7-9 – tectonic disturbances represented by crushing zones; 10 –breccia zones; 11 – Early Precambrian migmatized metamorphic rocks; 12 – target horizon of depository location; 13 – deep wells and their numbers; 14 – sampling points for detailed laboratory testing.

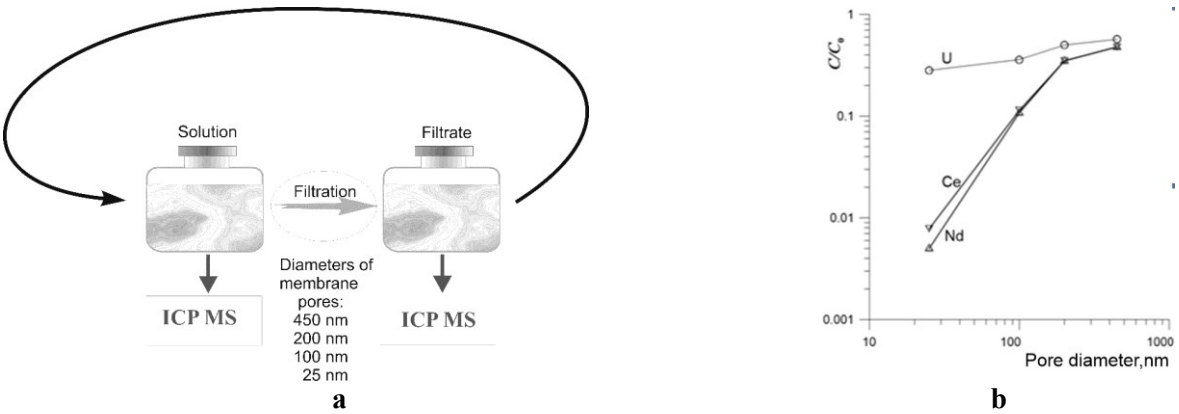

Fig 4. The analysis scheme (a) and the dependence of the concentrations of uranium and Ln-actinide imitator in the filtrate on the pore diameter (b). C_0— their initial concentration in the solution prior to filtration**.**

The size distribution of these particles was determined by sequentially filtration of the leaching solution through membranes with progressively reducing pore diameters (450, 200, 100, and 25 nm) (Fig. 4). It was found that the bulk of the actinide imitators are contained in the composition of colloid particles ranging in size from 200 to 400 nm.

Previously, based on the Kozeny–Carman approximation, a theory was developed to estimate the size distribution of pore channels in rocks using the results of gas permeability measurements on rock samples under various pressures. Such measurements were carried out on the samples from the Yeniseisky site, prepared from the core material taken from the near field of the repository (borehole P12, sampling depth — 496 m).

The measurements were carried out using a modified pulse decay method [Malkovsky et al., 2009]. The method is based on a comparison of the experimental data with the analytical and numerical solutions of the filtration equation, obtained taking into account the changes in viscosity and compressibility of the filtered gas at the given temperature and pressure. The measurement procedure is as follows.

One of the sections of the cylindrical sample is connected to a closed reservoir, while the other one is freely open to the atmosphere. At the initial moment of time, conventionally taken as zero, argon is supplied in the reservoir, resulting in an increase in the volume's pressure by Δp. Due to argon filtration through the sample to atmosphere, the pressure in the closed reservoir $p_{in}(t)$ gradually decreases from $p_{in}(t) + \Delta p$ to atmospheric p_{atm}. The sample permeability is determined by the rate of pressure reduction. The distribution of argon pressure in the sample satisfies the equation

$$\varphi\rho\frac{\partial p}{\partial t} = \frac{\partial}{\partial z}\left[\frac{\rho k_w}{\mu}\left(1+\frac{b}{p}\right)\frac{\partial p}{\partial z}\right], \quad (1)$$

where t– time; z– distance from the input section of the sample along its axis; ρ, μ– density and dynamic viscosity of argon; k_w – permeability of the sample for water; b – Klinkenberg parameter.

The initial and boundary conditions for equation (1) are as follows

$$t = 0, p = \begin{cases} p_{atm}, z > 0, \\ p_{atm} + \Delta p, z = 0 \end{cases}; \; z = 0, p = p_{in}(t); \; z = L, p = p_{atm} \quad (2)$$

where L– the length of the sample, $p_{in}(t)$ - the dependence determined by the condition of the argon mass balance in the input reservoir

$$V\frac{d\rho(p_{in})}{dt} = -\frac{Sk_w}{\mu(p_{in})}\left(1+\frac{b}{p_{in}}\right)\frac{\partial p}{\partial z}\Big|_{z=0}, \quad (3)$$

S, V – the cross-section of the sample and the input reservoir volume.

Equation (1), was integrated using the semi-implicit Crank-Nicolson method [Roach, 1980] taking into account conditions (2) and (3).

The argon density in the considered pressure and temperature range satisfies the equation of state for ideal gas. The viscosity was calculated using approximation relations for the viscous virial coefficients for argon [Zubarev et al., 1989].

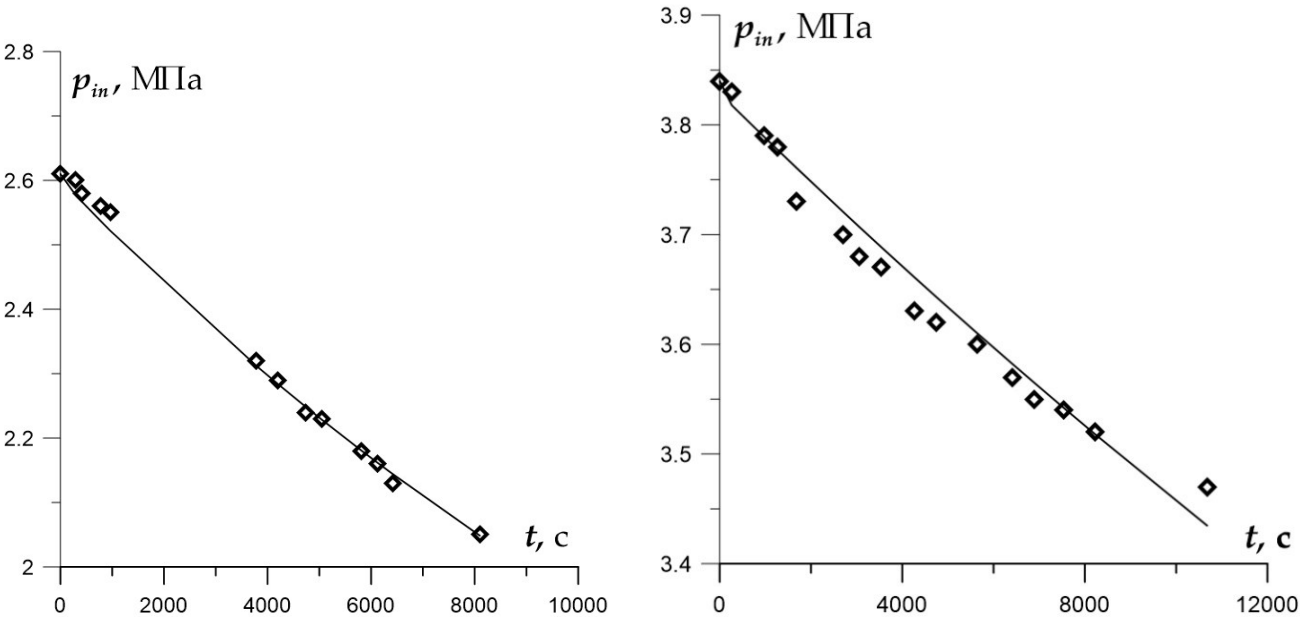

Fig. 5. Comparison of calculated and measured pressures for both studied samples.

The unknown k_w and b values were determined from the condition of the minimum function

$$F(k_w, b) = \sum_{i=1}^{N} [p_{in}(t_i) - p_i]^2,$$

where p_i –are the measured values $p_{in}(t_i), i = 1, \ldots, N$.

As a result of calculations the following values were obtained for the studied samples: (1) k_w= 2.29•10^{-20} m^2, b= 0.137 MPa; (2) k_w= 5.57•10^{-21} m^2, b= 0.0164 MPa. The comparison of the measured and calculated pressure values in the inlet reservoir at these values k_w and b for both samples is shown in Fig. 5 and demonstrates satisfactory agreement.

The permeability values obtained for the granite-gneisses of the «Yeniseisky» site, which, as mentioned above, is located in the framing of the Nizhnekansky massif, are comparable to those previously obtained for granitoids from the «Itatsky» and «Kamenny» sites, located directly within the massif (Figs. 1, 2) [Zharikov et al., 2014]. Based on the comparison of the size distributions of colloid particles and the pore channel diameters in the samples, it was found that 99.5 % of the colloidal particles will be retained mechanically in the rocks of the site.

The work was carried out within the framework of the State assignment of IGEM RAS.

References

1. Laverov N.P., Kantsel A.V., Lisitsin A.K., Omel'yanenko B.I., Pak A.A., Sel'tsov B.M., Filonenko Yu.D. The Main Tasks of Radioecology in Connection with the Disposal of Radioactive Waste. // Atomic Energy. 1991. V. 71. No. 6. Pp. 521-534 [in Russian].
2. Malkovsky V.I., Yudintsev S.V., Zharikov A.V. Radiocolloid Retention in the Nizhnekanskii Rock Massif // Doklady Earth Sciences. 2022. V. 503. P. 226–231. DOI: 10.1134/S1028334X22040109.
3. Malkovsky V.I., Zharikov A.V., Shmonov V.M. New Methods for Measuring the Permeability of Rock Samples for a Single-Phase Fluid // Izvestiya, Physics of the Solid Earth. 2009. V. 45. No. 2. P. 89–100.
4. Minaev V.A., Ozerskiy A.Yu., Poluektov V.V., Petrov V.A., and Murashov K.Yu. Petrography and Petrochemistry of Metamorphic and Igneous Rocks of the "Yeniseyskiy" Site // Russian Journal of Earth Sciences. 2026. V.26. ES1010. doi:10.2205/2026ES001063
5. Roache P.J. Computational Fluid Dynamics Albuquerque: Hermosa Publishers, 1976 446 p.
6. Thermophysical Properties of Technically Important Gases at High Temperatures and Pressures: A Handbook, Ed. by Zubarev V.N., Kozlov A.D., Kuznetsov V.M., et al., Moscow: Energoatomizdat, 1989 [in Russian].
7. Zharikov A.V., Velichkin V.I., Malkovsky V.I., Shmonov V.M. Experimental study of crystalline rock permeability: implications for underground radioactive waste disposal. // Water Resources. 2014. V.41. P. 881–895. doi:10.1134/S0097807814070136